



Hydrolysis of peptidoglycan is modulated by amidation of *meso*-diaminopimelic acid and Mg^{2+} in *Bacillus subtilis*

Alex Dajkovic ^{1,*} Benoit Tesson,¹
Smita Chauhan,¹ Pascal Courtin,¹ Ruth Keary,¹
Pierre Flores,¹ Christian Marlière,²
Sérgio R. Filipe ³ Marie-Pierre Chapot-Chartier¹
and Rut Carballido-Lopez^{1*}

¹MICALIS, INRA, AgroParisTech, Université Paris-Saclay, Jouy-en-Josas 78350, France.

²ISMO, UMR CNRS 8214, Université Paris Sud, Orsay Cedex 91405, France.

³Departamento de Ciências da Vida, Faculdade de Ciências e Tecnologia, Universidade Nova de Lisboa, Caparica 2829-516, Portugal.

Summary

The ability of excess Mg^{2+} to compensate the absence of cell wall related genes in *Bacillus subtilis* has been known for a long time, but the mechanism has remained obscure. Here, we show that the rigidity of wild-type cells remains unaffected with excess Mg^{2+} , but the proportion of amidated *meso*-diaminopimelic (mDAP) acid in their peptidoglycan (PG) is significantly reduced. We identify the amidotransferase *AsnB* as responsible for mDAP amidation and show that the gene encoding it is essential without added Mg^{2+} . Growth without excess Mg^{2+} causes $\Delta asnB$ mutant cells to deform and ultimately lyse. In cell regions with deformations, PG insertion is orderly and indistinguishable from the wild-type. However, PG degradation is unevenly distributed along the sidewalls. Furthermore, $\Delta asnB$ mutant cells exhibit increased sensitivity to antibiotics targeting the cell wall. These results suggest that absence of amidated mDAP causes a lethal deregulation of PG hydrolysis that can be inhibited by increased levels of Mg^{2+} . Consistently, we find that Mg^{2+} inhibits autolysis of wild-type cells. We suggest that Mg^{2+} helps to maintain the balance between PG synthesis and hydrolysis in cell wall mutants where this balance is perturbed in favor of increased degradation.

Accepted 15 March, 2017. *For correspondence. E-mail alexdajkovic@gmail.com. OR E-mail rut.carballido-lopez@inra.fr; Tel: +33 (0)1 34 65 29 55; Fax: +33 (0)1 34 65 25 21.

Introduction

Bacterial cell walls are exoskeletal macromolecular structures that protect cells and give them shape and mechanical integrity. Their physiology is characterized by a delicate balance between rigidity, which confers mechanical stability and plasticity, which permits growth and division. The physical basis of the rigidity of bacterial cell walls is a network of polymers whose dominant component is the peptidoglycan (PG) (Turner *et al.*, 2014). The PG meshwork (the sacculus) is composed of linear strands of glycan chains crosslinked via peptide stems. Glycan chains are universally composed of repeating units of β -(1,4) linked N-acetyl glycosamine and N-acetyl muramic acid (Turner *et al.*, 2014). The stem peptides vary between species and are used as a taxonomic criterion for classifying bacteria (Schleifer and Kandler, 1972). They are synthesized as pentapeptide chains containing unconventional D-amino acid residues attached to the lactyl moiety of muramic acid, and possess a di-basic amino acid in the third position. *Meso*-diaminopimelic acid (mDAP) is characteristic of Gram-positive bacilli and most Gram-negative species, L-Lys of the majority of Gram-positive organisms and L-Orn of Spirochetes (Vollmer *et al.*, 2008a). In the rod-shaped Gram-positive model organism *Bacillus subtilis* the pentapeptide consists of L-Ala-D-iso-Glu-mDAP-D-Ala-D-Ala (Atrih *et al.*, 1999). Gram-positive cell walls further contain carbohydrate-based anionic polymers, primarily teichoic acids, which account for roughly half of the mass of the cell wall. Their physiological functions remain elusive but they play a major role in divalent cation binding (particularly Mg^{2+}) (Brown *et al.*, 2013; Neuhaus and Baddiley, 2003; Heckels *et al.*, 1977), they serve as scaffolds for a wide range of molecules and they regulate cell wall-associated enzymes (Yamamoto *et al.*, 2008; Brown *et al.*, 2013).

Plasticity of PG depends upon systems of enzymes with opposing activities. On the one hand, synthetic enzymes make and interlink new glycan chains, and, on the other hand, hydrolytic enzymes cut existing bonds to permit growth and remodeling (Turner *et al.*, 2014). High-molecular-weight penicillin binding proteins (PBPs) are membrane-embedded PG-synthesizing enzymes

that possess transglycosylase and/or transpeptidase activities. In *B. subtilis*, PG degradative enzymes, termed PG hydrolases, are numerous and highly redundant (Smith *et al.*, 2000; Vollmer *et al.*, 2008b). They possess a range of hydrolytic activities including recognizing and cutting the bonds between the sugar moieties in the glycan chain (glucosaminidases and muramidases/lytic transglycosylases), between N-acetyl muramic acid and the peptide stem (amidases) and between specific amino acids in the peptide stems or in the peptide bridges (endopeptidases) (Smith *et al.*, 2000). Uncontrolled activity of PG hydrolases could compromise cellular integrity and lead to lysis. Indeed, some PG hydrolases are autolysins that can lyse growing cells when their proton motive force (*pmf*) is dissipated by depolarization of the membrane by chemical uncouplers, such as azide or CCCP, or by starvation (Jolliffe *et al.*, 1981; Lamsa *et al.*, 2012). In *B. subtilis*, the autolysins are the amidase LytC, the glucosaminidase LytD, and the DL-endopeptidases LytE and LytF (Smith *et al.*, 2000). Cells of the mutant strain where genes encoding these four autolysins are absent do not undergo lysis upon dissipation of the *pmf*, but they still grow and divide, indicating that other PG hydrolases can confer plasticity to the cell wall for these purposes (Lamsa *et al.*, 2012). The rest of the putative PG hydrolase complement of *B. subtilis* includes more than 30 enzymes (Smith *et al.*, 2000) that are not autolysins and are often enmeshed in complex regulatory networks (Meisner *et al.*, 2013). Overall, and despite the important role of PG hydrolases in cell wall metabolism, their regulation remains largely unknown.

In rod-shaped bacteria, the coordination of PG synthesis and degradation results in controlled cell wall enlargement and division, and produces cells with narrowly defined cell dimensions for a given growth condition. This coordination is effected by two complementary PG-synthesizing systems that are associated with cytoskeletal elements, and control sidewall elongation and septation respectively. The system involved in cell division is governed by the bacterial tubulin FtsZ and the associated septation-specific PBPs. The system involved in sidewall elongation is controlled by the Rod system, a system of morphogenetic proteins including the bacterial actin homologue MreB as well as MreC, MreD, RodA, RodZ and elongation-specific PBPs (Eun *et al.*, 2015). One of the unexplained aspects of the Rod system in *B. subtilis* is that the lethality and/or morphological defects of the absence of some of its components can be overcome by adding Mg^{2+} to the growth medium (Formstone and Errington, 2005). *mreB* and its paralog *mbi* are essential in standard laboratory conditions. However, when growth media are supplemented with 5–25 mM Mg^{2+} , *mreB* and *mbi* mutants grow and

divide normally and assume a normal rod-shaped morphology. When Mg^{2+} is depleted, the morphological phenotype becomes manifest and they grow as deformed and ballooning cells before eventually lysing (Formstone and Errington, 2005; Chastanet and Carballido-Lopez, 2012). Mg^{2+} likewise suppresses the viability and/or morphological defects of several other cell wall related mutants (e.g. *mreC*, *mreD*, *ponA*, *ugtP*, *pgcA* or *gtaB*) (Murray *et al.*, 1998; Chastanet and Carballido-Lopez, 2012), but the mechanism underlying this rescuing role is currently unknown. Two main hypotheses have been put forth to explain it. It has been suggested that Mg^{2+} may have a structural role in enhancing the rigidity of the cell wall or, alternatively (or simultaneously), a regulatory role by affecting the activity of cell-wall embedded enzymes (Formstone and Errington, 2005). It has been known for several decades that Mg^{2+} binds to cell walls of Gram-positive bacteria (Beveridge and Murray, 1980; Heckels *et al.*, 1977). Recent solid state NMR studies estimate the dissociation constant at approximately 0.6 mM (Kern *et al.*, 2010).

One of the ways bacteria can regulate the metabolism of their cell walls is by chemical modification of the constituent subunits. For example, a common modification is the deacetylation of N-acetyl glucosamine. This modification abolishes the binding of LysM domain containing proteins, such as some autolysins and PG hydrolases, and may thereby modulate their activity (Mesnage *et al.*, 2014). A distinct and widespread modification is the O-acetylation of N-acetyl muramic acid, which is associated to resistance to lysozyme and endogenous autolysis, as well as to resistance to penicillin and macrophage killing (Bernard *et al.*, 2011a; Davis and Weiser, 2011). Another common modification, only present in Gram-positive organisms, is the amidation of carboxyl groups of amino acids in the stem peptides or peptide cross-bridges. Commonly amidated are the α -carboxyl of the D-Glu in the second position of the stem peptide, and the ϵ -carboxyl group of the mDAP in the third position. In *Staphylococcus aureus* and *Streptococcus pneumoniae* where the di-basic amino acid is L-Lys instead of mDAP, D-Glu is amidated to D-iso-glutamine. The two enzymes responsible for D-Glu amidation (the MurT/GatD complex) have been identified (Munch *et al.*, 2012; Figueiredo *et al.*, 2012), and PG transpeptidases have been shown to work more efficiently when D-Glu is amidated (Munch *et al.*, 2012; Figueiredo *et al.*, 2012). In *B. subtilis*, mDAP was found to be amidated in most muropeptides of vegetative cell PG, while D-Glu was not amidated (Atrih *et al.*, 1999; Warth and Strominger, 1971). Amidation of mDAP has also been found in PG of other bacteria (Bernard *et al.*, 2011b; Schleifer and Kandler, 1972; Levefaudes *et al.*, 2015; Mahapatra

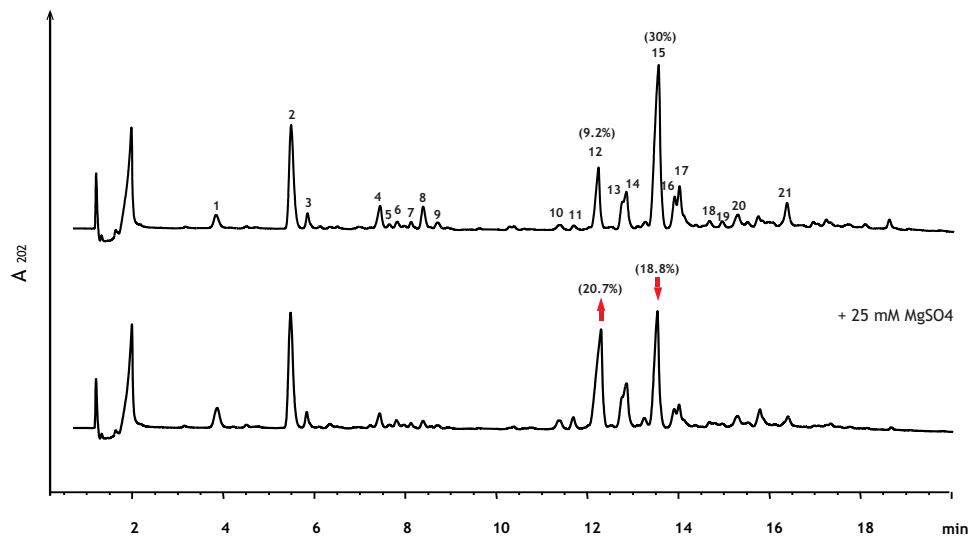


Fig. 1. Effect of Mg^{2+} on muropeptide composition of vegetative PG of wild-type *B. subtilis*. RP-UPLC separation of muropeptides released by mutanolysin digestion of PGs extracted from *B. subtilis* wild-type strain BSB1 grown in PAB in the absence (upper chromatogram) and in the presence of 25 mM $MgSO_4$ (lower chromatogram). The major muropeptide dimer peaks with only one (peak 12) or two (peak 15) amidated mDAP moieties are indicated by the red arrow pointing up and down respectively (their percentages of total muropeptide are indicated in parentheses above the peaks). Supporting Information Table 1 lists the masses and the identities of the numbered peaks.

et al., 2005). AsnB1 and LtsA were recently identified as the amidotransferases responsible for mDAP amidation in *Lactobacillus plantarum* (Bernard *et al.*, 2011b) and *Corynebacterium glutamicum* (Levefaudes *et al.*, 2015) respectively. These proteins belong to a large family of glutamine amidotransferases (Raushel *et al.*, 1999), which catalyze the transfer of ammonia from glutamine to various substrates. A canonical member of this family is the asparagine synthase of *Escherichia coli*, AsnB (Huang *et al.*, 2001). PG recognition by the mammalian host innate immune system has been shown to be affected by amidation of mDAP (Asong *et al.*, 2009; Girardin *et al.*, 2003) but the physiological role of mDAP amidation in the homeostasis of the bacterial cell wall remains unknown. PG synthesizing enzymes seem to work as efficiently on amidated as in non-amidated mDAP in both *L. plantarum* and *C. glutamicum* (Bernard *et al.*, 2011b; Levefaudes *et al.*, 2015), suggesting that mDAP amidation may not be necessary for efficient cell wall synthesis (Levefaudes *et al.*, 2015; Hirasawa *et al.*, 2000). However, in *L. plantarum* *asnB1* seems to be essential and the mutant strains are affected in growth and morphology (Bernard *et al.*, 2011b).

In this work, we describe the differential amidation of mDAP as an important chemical modification of the PG of *B. subtilis* wild-type cells grown in the presence of high concentrations of Mg^{2+} . We identified AsnB as the enzyme responsible for catalyzing it, and characterized the phenotype of mutant cells. Our results suggest that both Mg^{2+} and amidation of mDAP are involved in modulating PG hydrolysis.

Results

*Excess extracellular Mg^{2+} causes a decrease in amidation of mDAP in *B. subtilis**

To gain insight into the effect of magnesium on the cell wall, we examined the muropeptide composition of the PG of wild-type *B. subtilis* cells grown in PAB (Penassay broth) in the absence and in the presence of 25 mM $MgSO_4$. The muropeptide profiles (Fig. 1) were similar to those previously reported for the PG of vegetative cells grown in LB medium (Atrih *et al.*, 1999). When no Mg^{2+} was added, uncleaved dimeric muropeptides containing amidation on both mDAP moieties represented 34% of all muropeptides, while muropeptide dimers with amidation on only one mDAP represented 14% of all muropeptides (the major dimer peaks 12 and 15 are indicated by red arrows in Fig. 1 and highlighted in grey in Supporting Information Table 1). In contrast, cells grown with excess Mg^{2+} had only 21.6% of dimeric muropeptides with doubly amidated mDAP, while the dimers containing only one amidation represented 23% of all identified muropeptides (Fig. 1 bottom panel, and Supporting Information Table 1). This corresponds to greater than 60% increase of singly amidated dimers in cells grown in the presence of added Mg^{2+} . The effect was identical in different growth media (Fig. 1 for PAB medium, Supporting Information Fig. S1A and B for LB medium), and it was independent of the wild-type strain used. Data for the strain BSB1 are shown in Fig. 1 and Supporting Information Fig. S1A and B; data for the strain 168_{ed} in Supporting Information Fig. S1C and D.

To test whether this effect was produced by a generic increase in the ionic strength in the medium, cells were grown in the presence of 100 mM NaCl. This concentration of NaCl has the same ionic strength as 25 mM MgSO₄, since $I = \frac{1}{2} \sum_{i=1}^n c_i z_i^2$, where I is the ionic strength, c_i is the molar concentration of ion i and z_i is the charge number of that ion. In contrast to cells grown in the presence of high Mg²⁺, cells grown in medium supplemented with NaCl did not show any changes in the degree of amidation of dimeric muropeptides, nor any other significant change in the muropeptide profile (Supporting Information Fig. S1E). This indicated that Mg²⁺ specifically affected the level of amidated mDAP in *B. subtilis* PG.

In addition, we used atomic force microscopy (AFM) to measure the rigidity of the cell wall of living cells in the presence of Mg²⁺. Excess extracellular Mg²⁺ had no effect on the rigidity of the cell wall of live hydrated cells (representative cell are shown in Supporting Information Fig. S2B and D). The Young modulus was 40.2 ± 4.9 MPa for cells grown without supplemented Mg²⁺ and 39.7 ± 4.6 MPa for cells in the presence of 25 mM MgSO₄. The topography of cell surfaces likewise remained unchanged (Supporting Information Fig. S2A and C), suggesting that excess Mg²⁺ does not affect the structure and mechanical properties of the cell wall.

asnB, *asnH*, *asnO* are homologues of mDAP amide transferases from *L. plantarum* and *C. glutamicum*

We sought to identify the amidotransferase responsible for amidation of mDAP in *B. subtilis*. BLAST search analysis using the amino acid sequences of AsnB1 from *L. plantarum* and LtsA from *C. glutamicum*, revealed three homologues in *B. subtilis* strain 168: AsnB, AsnH and AsnO (Supporting Information Fig. S3). Their homology with *C. glutamicum* LtsA has E values below 10e⁻⁵¹ with identities ranging from 23% for AsnH, 31% for AsnO and 56% for AsnB. Similarly, the homologies with *L. plantarum* AsnB1 are high, with E values below 10e⁻⁴⁸ and identities at 28% for AsnH and AsnO and 50% for AsnB. The *ansB*, *asnH* and *asnO* gene products were previously predicted to be asparagine synthetases on the basis of the amino acid sequence similarity to AsnB of *E. coli*, to which they are all three orthologous to the same extent (~ 28% similarity) (Yoshida *et al.*, 1999). Each of the three genes complemented an *E. coli* strain lacking asparagine synthetases, indicating that all encode enzymes capable of synthesizing asparagine (Yoshida *et al.*, 1999). However, while deletion of *asnO* and/or *asnH* in *B. subtilis* had no effect on growth, deletion of *asnB* was reported to lead to a slow-growth

phenotype even in the presence of high levels of asparagine (Yoshida *et al.*, 1999).

Mg²⁺-dependent growth of Δ *asnB* mutant strain

To investigate whether AsnB, AsnH and/or AsnO are involved in mDAP amidation in *B. subtilis*, we attempted to inactivate the corresponding genes by backcrossing their previously reported deletions (Yoshida *et al.*, 1999) into our BSB1 wild-type reference laboratory strain. *asnH* and *asnO* null mutants were readily obtained. The colonies of the resulting strains had normal rugose morphology and grew as well as the wild-type strain. In contrast, the strain carrying a deletion of *asnB* (*asnB::neo*) could not be reliably obtained using unsupplemented growth media. Backcrossing the *asnB::neo* allele gave variable results that were not reproducible between experiments. Sometimes the few neo^R transformants produced colonies of different sizes with some being smooth and others rugose, and sometimes no transformants were obtained. This suggested that *asnB* is essential in *B. subtilis*, like *asnB1* in *L. plantarum* (Bernard *et al.*, 2011b), and that suppressor mutations arise to alleviate the growth defect associated with the loss of AsnB. To test if *asnB* plays an essential role in the homeostasis of the cell wall, we tested whether high levels of Mg²⁺ were able to compensate this defect and permit reliable transformation. In the presence of 25 mM Mg²⁺, we readily obtained colonies of the same size with homogeneously smooth appearance, giving the strain BDA33 (*asnB::neo*). We were similarly able to construct a triple mutant strain carrying deletions in *asnB*, *asnH*, and *asnO* (BDA329).

The Δ *asnB* mutant was not able to grow on PAB plates (~210 μ M Mg²⁺) on which the wild-type grew normally. Even though AsnB is annotated as an asparagine synthase, addition of asparagine to the medium did not permit the restoration of growth under our experimental conditions (Fig. 2A). However, growth was completely restored when the plates were supplemented with 25 mM Mg²⁺ (Fig. 2A). Growth of the Δ *asnB* mutant was also Mg²⁺-dependent in liquid media (Fig. 2B and C for PAB medium, and Supporting Information Fig. S4 for LB). In PAB supplemented with 5 mM Mg²⁺, the mutant grew at significantly slower rate than the wild-type, and at ≥ 10 mM Mg²⁺ it grew as well as the wild-type strain (Fig. 2B and C). Taken together, these results show that *asnB* is essential in media without additional Mg²⁺, suggesting that AsnB has a cell wall related function in addition to its previously reported asparagine synthetase activity (Yoshida *et al.*, 1999).

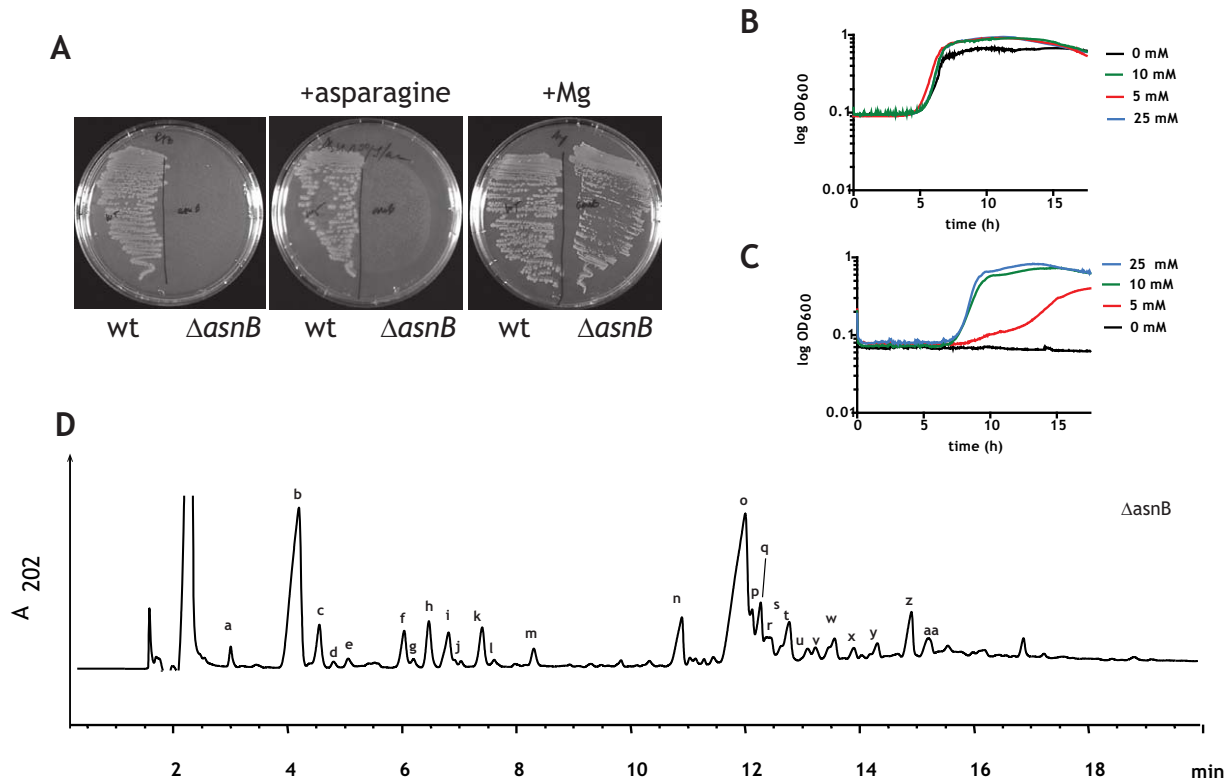


Fig. 2. Conditional lethality and muropeptide analysis of Δ *asnB* mutant strain.

A. Wild-type *B. subtilis* BSB1 and Δ *asnB* (BDA33) strains were streaked on PAB plates unsupplemented (left panel) and supplemented with 100 μ g ml⁻¹ of L-asparagine (central panel) or with 25 mM MgSO₄ (right panel).

B. and C. Growth curves of the wild-type strain (B) and the Δ *asnB* mutant (C) grown at 37°C in PAB medium supplemented of the indicated concentrations of MgSO₄. D. RP-UPLC separation of muropeptides extracted from vegetative PG of the Δ *asnB* (strain BDA33) grown in PAB supplemented with 25 mM MgSO₄. The numbered peaks were identified by MALDI-TOF and are shown in Supporting Information Table 2.

Complete absence of amidated mDAP in the peptidoglycan of Δ *asnB* mutant cells

To examine the involvement of AsnB, AsnH and AsnO in amidating mDAP, we studied the chemical composition of the PG of the mutant strains grown in the presence of excess Mg²⁺. Muropeptide profiles of the wild-type, Δ *asnH*, and Δ *asnO* mutant strains were indistinguishable (Supporting Information Fig. S5). In contrast, the Δ *asnB* mutant strain (Fig. 2D) displayed a strikingly different muropeptide profile, with a general shift of all major peaks to lower retention times. This is particularly evident for the major monomer (peak b in Fig. 2D) and dimer (peak o in Fig. 2D) peaks. This was consistent with the absence of amidation of the ϵ -carboxyl of mDAP since the non-amidated forms of mDAP-containing muropeptides are less hydrophobic and thus their retention on the reverse phase (C₁₈) column is reduced. Consistently, mass-spectrometry revealed masses in accordance with complete absence of amidation on mDAP in the Δ *asnB* mutant (Supporting Information Table 2).

The calculated crosslinking index of the Δ *asnB* mutant (39%) was similar to that of the wild-type (40%) and

consistent with previously published estimates (Atrih *et al.*, 1999). This indicated that PG synthetic enzymes involved in transpeptidation are capable of accepting non-amidated forms of mDAP as substrate as efficiently as the amidated forms.

Altogether, these results show that AsnB is indispensable for amidation of mDAP in *B. subtilis* and suggest involvement of this chemical modification in cell wall metabolism. The link with cell wall metabolism is further reinforced by the correlation of expression of *asnB* with cell wall metabolism genes in approximately 200 different growth conditions (Nicolas *et al.*, 2012). All but two of the first twenty genes which are most correlated with *asnB* are involved in cell wall metabolism, which is not the case for *asnH* or *asnO* (<http://genome.jouy.inra.fr/cgi-bin/seb/index.py>).

Depletion of Mg²⁺ causes deformation and cell lysis in Δ *asnB* mutant cells

In the presence of high concentrations of Mg²⁺ the ultrastructure of the cell envelope of Δ *asnB* mutant cells was not appreciably different from that of wild-

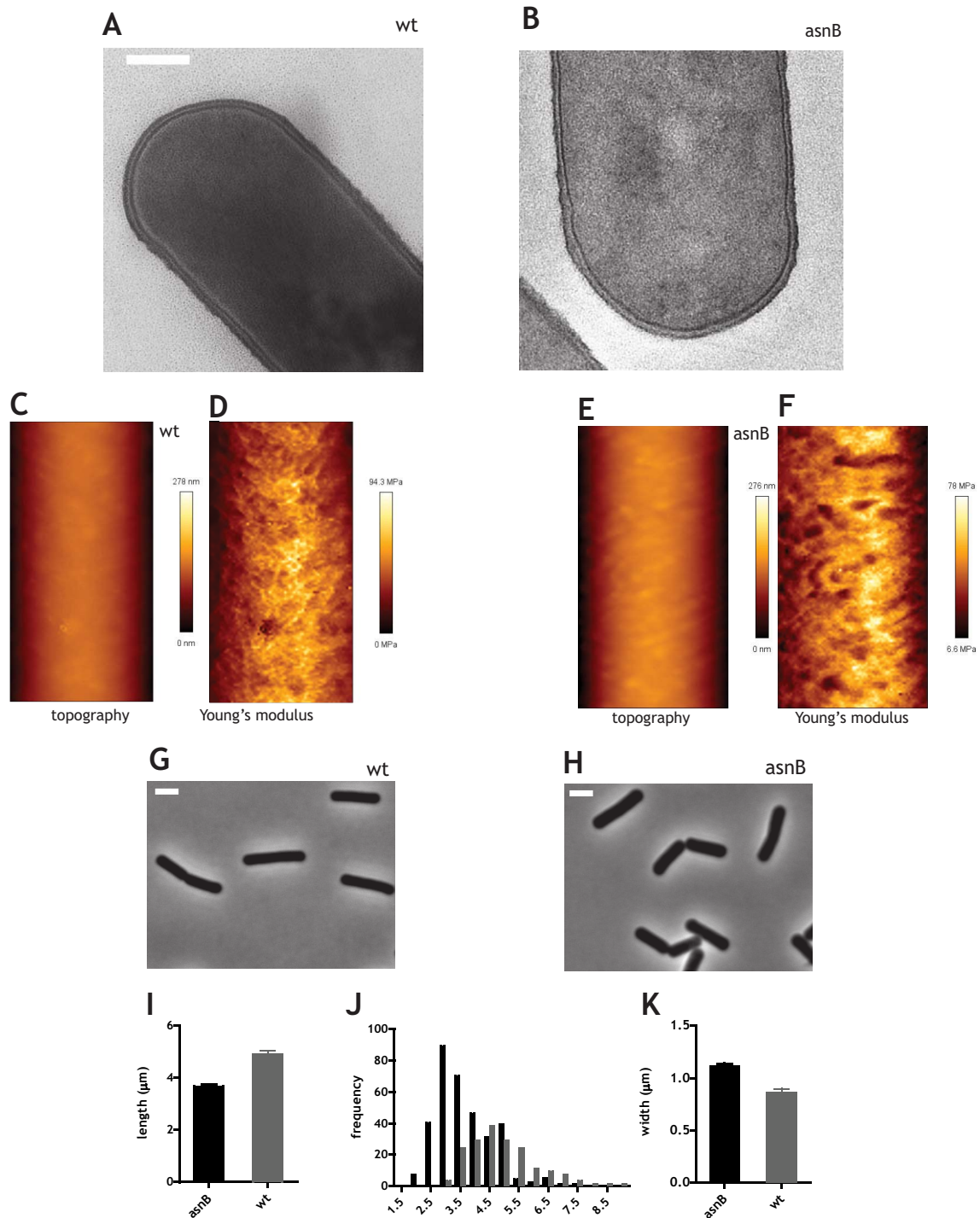


Fig. 3. Ultrastructure, mechanics, and morphology of $\Delta asnB$ mutant cells grown with excess Mg^{2+} . Cells were grown to mid-exponential phase in LB medium supplemented with 25 mM Mg^{2+} .

A. and B. Transmission electron micrographs of wild-type (A) and $\Delta asnB$ (B) cells. Scale bar is 200 nm.

C–F. Atomic force microscopy imaging of the surface topography (C and E) and of rigidity measurement (D and F) of wild-type (C and D) and $\Delta asnB$ mutant cells (E and F). Scale of height is indicated to the right of panels C and E and the scale of Young's modulus is indicated on the right of panels D and F. Scan size was 0.683 by 1.711 μm .

G and H. Phase-contrast micrographs of wild-type (G) and $\Delta asnB$ cells (H). Scale bar is 2 μm .

I. Bar graph of average cell length of wild-type and $\Delta asnB$ cells. 95% confidence intervals are shown (> 300 cells were measured). J. Histogram of cell lengths for wild-type and $\Delta asnB$ mutant cells. K. Bar graph of width of wild-type and $\Delta asnB$ mutant cells. 95% confidence intervals are shown (> 300 cells were measured).

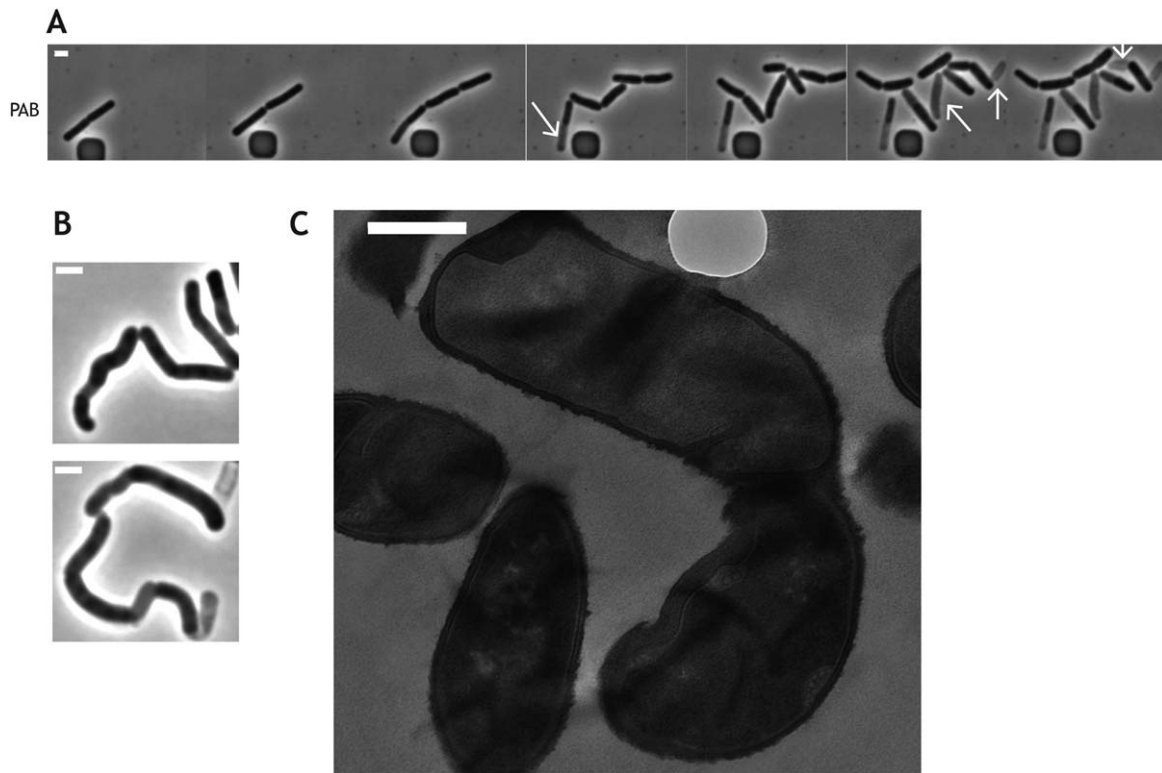


Fig. 4. Depletion of excess Mg^{2+} causes cell deformation and lysis of $\Delta asnB$ cells.

A. Time-lapse microscopy capturing the phenotype of $\Delta asnB$ cells after removal of Mg^{2+} in PAB. Cells of strain BDA33 (*asnB::neo*) were grown in the microfluidics device under continuous flow of PAB medium supplemented with 25 mM $MgSO_4$. The flow was stopped, the microfluidic chamber was flushed with unsupplemented medium and the cells were allowed to resume growth in unsupplemented medium. Cells were imaged every 20 seconds (every 80th image is shown), for full movie see Supporting Information Movie 1. White arrows indicate lysing cells. Scale bar, 2 μm .

B. Phase-contrast micrographs of $\Delta asnB$ cells grown in LB medium in the presence of limiting concentrations of Mg^2 . Top panel, 1 mM $MgSO_4$; bottom panel, 5 mM $MgSO_4$. Scale bar, 2 μm

C. Ultrastructure of $\Delta asnB$ cells grown in LB without added Mg^{2+} examined by transmission electron microscopy. Scale bar is 500 nm.

type cells (Fig. 3A and B). Similarly, their cell surface topography and their rigidity were comparable to those of wild-type cells when assayed by AFM (Fig. 3C–F). The rigidity of wild-type was 39.7 ± 4.6 MPa versus 41.6 ± 3 MPa for $\Delta asnB$ mutant, suggesting that the absence of mDAP amidation did not affect the structural integrity and mechanics of the cell wall. $\Delta asnB$ mutant cells grown in the presence of 25 mM Mg^{2+} displayed normal rod shape (Fig. 3H), although they were significantly shorter (Fig. 3I and J) and wider (Fig. 3K) than wild-type cells (mean width was $1.1(\pm 0.05)$ μm and $0.85(\pm 0.07)$ μm respectively).

To investigate the phenotypes suppressed by the presence of excess Mg^{2+} , we used time-lapse microscopy. Cells were grown in a microfluidic device in either PAB or LB medium supplemented with 25 mM Mg^{2+} and microscopically followed after removal of Mg^{2+} . When unsupplemented PAB medium was flowed through the microfluidic device, cells lacking *AsnB* grew for approximately one cell

cycle and subsequently started to deform and rapidly lyse (Fig. 4A, Supporting Information Movie 1). Mutant cells grown in batch culture in the presence of limiting concentrations of Mg^{2+} displayed similar lytic phenotype and morphological defects, with inhomogeneities in their diameter and an undulating appearance of the sidewalls (Fig. 4B). Local thickening of the cell wall was observed in some deformed cells (Fig. 4C). When Mg^{2+} depletion occurred in LB, where the concentration of Mg^{2+} is higher than in PAB but still too low to support normal growth of the $\Delta asnB$ mutant strain (see above and Supporting Information Fig. S4), growth continued for several cell cycles. The morphological deformations that accompanied growth were more pronounced (Fig. 6B upper row of panels, Supporting Information Movie 3), presumably because cells grew longer before lysing. The most remarkable morphological change was the increase in cell diameter and the appearance of bulges (Fig. 6B and Supporting Information Movie 3).

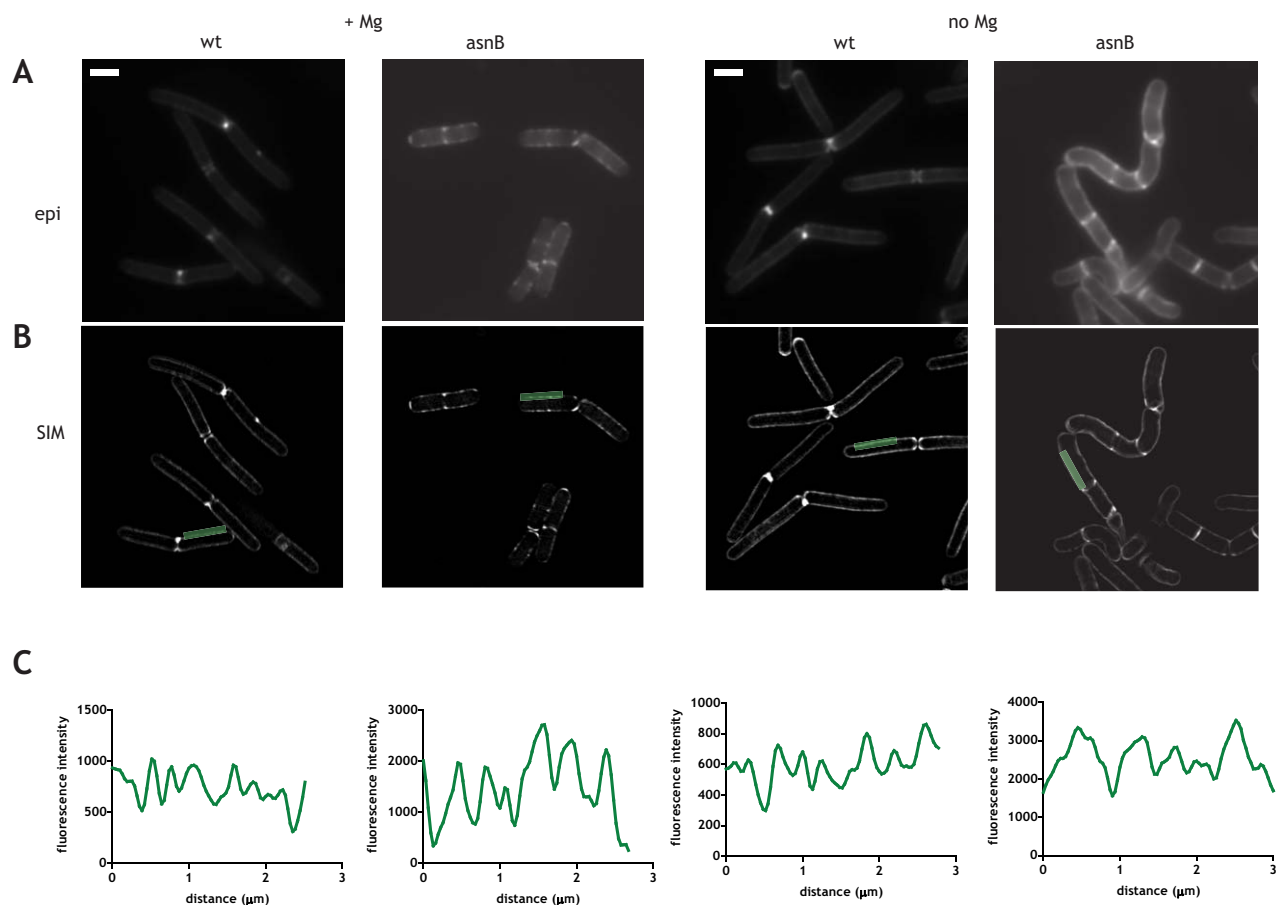


Fig. 5. Isotropic insertion of PG along the sidewalls of the wild-type and Δ asnB mutant cells. Epifluorescence (A) and structured illumination microscopy (B) imaging of insertion of peptidoglycan by TDL labeling in the presence of added Mg^{2+} (two panels on the left) and in the absence of added Mg^{2+} (two panels on the right). Structured illumination microscopy (SIM) images of the medial plane of the cell are shown. C. Quantification of fluorescence along the green line shown in SIM images. For SIM images of additional cells see Supporting Information Fig. S6.

In contrast, wild-type cells grew and divided normally in the microfluidic device (Fig. 6A and Supporting Information Movie 2).

Ordered insertion of peptidoglycan in the sidewall of the Δ asnB mutant

The cell deformations in the Δ asnB mutant could be produced by deregulated PG synthetic activity, by uncontrolled PG hydrolysis, or by both. To determine whether cell deformations caused by the absence of AsnB were accompanied by normal PG synthesis, we visualized PG insertion in Mg^{2+} -depletion experiments using TAMRA red D-lysine (TDL) (Kuru *et al.*, 2012, 2015) by incubating cells + for 1/4 of cell doubling time (5–6 minutes). This non-toxic fluorescent D-amino acid derivative is incorporated in the fifth position of the stem peptide in *B. subtilis* (Kuru *et al.*, 2012). TDL labeling of wild-type cells produced a regular punctuate fluorescent

pattern along the sidewall, revealing the sites of PG insertion (Fig. 5A), as previously described (Kuru *et al.*, 2012, 2015). This punctuate labeling was observed in either the presence or the absence of Mg^{2+} (Fig. 5A). Super-resolution imaging of the TDL-labeled cells by structured illumination microscopy (SIM) confirmed the regularity of the pattern along the length of the cell (Fig. 5B and C). Peaks of fluorescence, corresponding to the sites of PG insertion, were evenly distributed with an average spacing between approximately 0.5 and 1 μ m, consistent with the reported spacing between the tracks followed by MreB-associated PG synthetic machineries along the sidewalls of *B. subtilis* (Dominguez-Escobar *et al.*, 2011; Garner *et al.*, 2011).

Very similar labeling was observed for Δ asnB mutant cells, whether they were grown in the presence or in the absence of Mg^{2+} (Fig. 5). Even in the zones where Δ asnB cells were becoming deformed, there were no notable differences of the distribution of the fluorescent

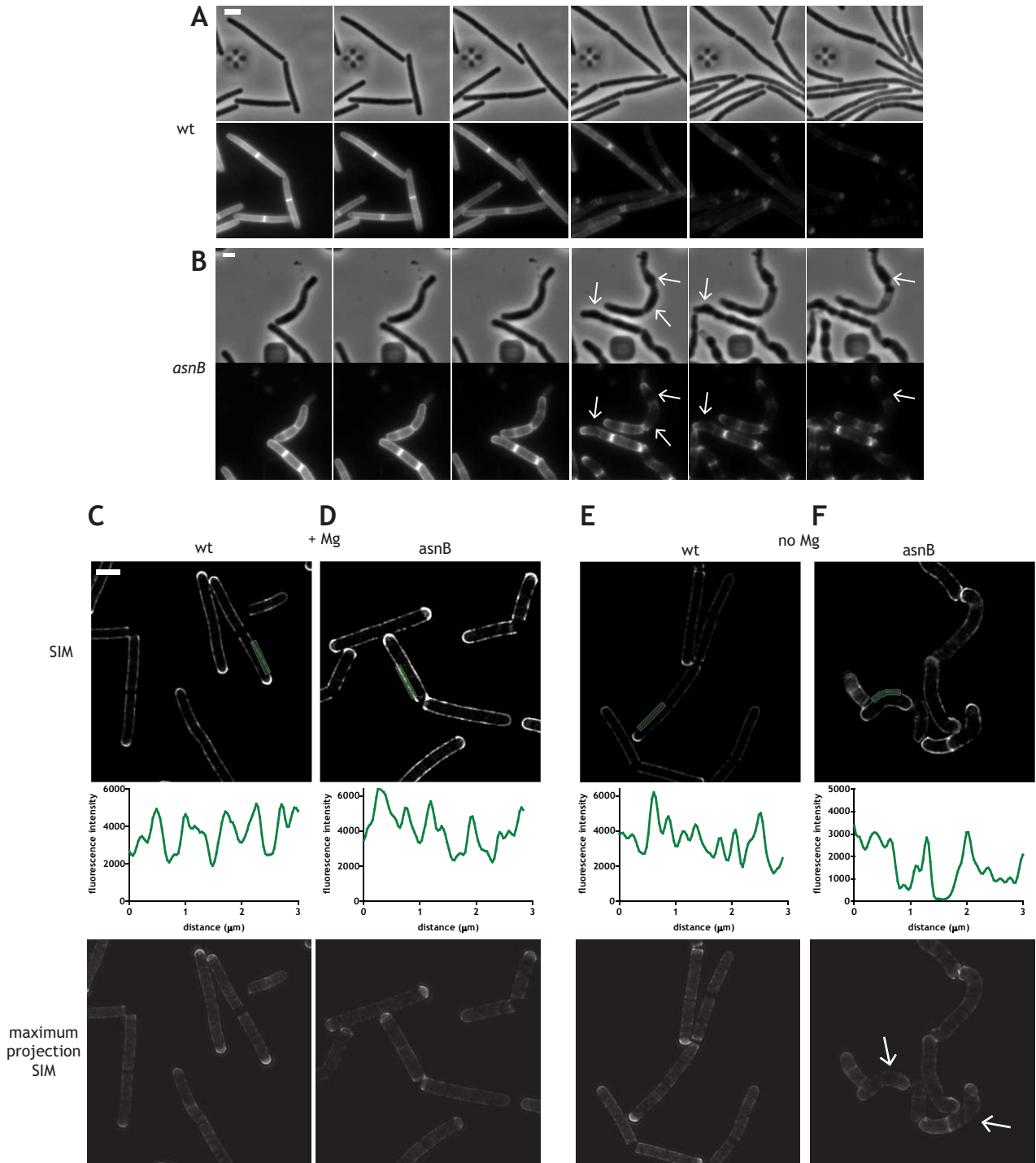


Fig. 6. Imaging of depletion of TDL label in growing cells.

A. and B. Time-lapse pulse-chase experiments in a microfluidic device (CellAssic). Disappearance of the TDL label from the PG of wild-type (A) and Δ asnB mutant cells (B) during growth in LB without added Mg²⁺. Images were taken every 5 minutes (every third image is shown in the panels) after a 20 minute labeling pulse done in the presence of added Mg²⁺. Phase contrast images are shown above of their corresponding fluorescence images. Deformations of cells and the corresponding anisotropic loss of the label in the Δ asnB mutant are indicated by white arrows. See also Supporting Information Movies 2 and 3. Scale bars, 2 μ m.

C–F. SIM images of the depletion of TDL label in batch cultures of the wild-type (C and E) and the Δ asnB mutant (D and F) grown in LB medium in the presence (C and D) and in the absence (E and F) of 25 mM MgSO₄. SIM images of the medial plane of the cell are shown in the upper panel, quantifications of fluorescence along the green line in SIM images are shown in the middle panel, and maximum projections of the SIM images are shown in lowest panels. White arrows in panel F indicate regions of significant loss of label. Scale bars, 2 μ m. Epifluorescence images corresponding to panels C to F are shown in Supporting Information Fig. S7.

signal with respect to other regions of the cell where there were no signs of deformations (Fig. 5 and Supporting Information Fig. S6).

In summary, PG synthesis assayed by TDL labeling was ordered in the wild-type and in the $\Delta asnB$ mutant, even under conditions which led to deformed cell morphology in the mutant. This suggested that the organization of PG synthesis is not defective in cells lacking AsnB and thus that the deformations may be caused by another mechanism.

Anisotropic peptidoglycan degradation in the $\Delta asnB$ mutant

We then investigated cell wall degradation that accompanies sidewall elongation using TDL pulse-chase microluidic experiments. Cells were labeled with TDL for one entire doubling time (~ 20 min) in the presence of added Mg^{2+} , washed, and the disappearance of the label was followed in real time allowing the cells to grow in fresh medium without added Mg^{2+} . We reasoned that the appearance of dark zones could indicate zones of PG degradation (either loss/breakup or turnover/maturation), and/or of new PG insertion. Since the pattern of PG synthesis was regular in the $\Delta asnB$ mutant (Fig. 5 and Supporting Information Fig. S6), the appearance of irregularities in the loss of fluorescence could therefore be attributed to anisotropic degradation of PG.

Growth of wild-type cells was accompanied by an isotropic loss of the TDL label (Fig. 6A, see also Supporting Information Movie 3). In contrast, loss of TDL label in the $\Delta asnB$ mutant was unevenly distributed (Fig. 6B). Fluorescence loss appeared concentrated in regions where the cells were beginning to deform and increase in diameter (white arrows in Fig. 6B, see also Supporting Information Movie 3). To quantify the loss of label along the sidewall, we performed a similar experiment in batch cultures and imaged the cells using SIM and epifluorescence after one quarter to one half of cell cycle of depletion (~ 10 min under these conditions). In the presence of excess Mg^{2+} , the disappearance of the label was isotropic in both wild-type cells and $\Delta asnB$ mutant cells (Fig. 6C and D respectively; see also Supporting Information Fig. S7A and B for the corresponding epifluorescence images). Fluorescence intensity profiles along the sidewalls showed evenly distributed gaps in fluorescence intensity whose average distance was again approximately $0.5\text{--}1\ \mu\text{m}$. (Fig. 6C and D), suggesting that such gaps corresponded to MreB-associated PG insertion and/or degradation. Wild-type cells displayed the same pattern of fluorescence loss upon Mg^{2+} depletion (Fig. 6E and Supporting Information Fig. S7C, see lower panel of Supporting Information

Fig. S7C for comparison of patterns obtained from SIM and epifluorescence images). In contrast, fluorescence intensity profiles along the sidewalls of $\Delta asnB$ mutant cells in the absence of supplemented Mg^{2+} showed extensive areas of loss of the TDL label which appeared more pronounced in zones where the cells were becoming deformed from their normal rod-shape morphology (Fig. 6F and Supporting Information Fig. S7D, see lower panel of Supporting Information Fig. S7D for comparison of patterns obtained from SIM and epifluorescence images). This is particularly obvious in 3D projections of SIM images where the entire cell body is more easily visualized (white arrows in Fig. 6F and Supporting Information Fig. S8).

Because PG insertion was regular in the $\Delta asnB$ mutant in the absence of Mg^{2+} even in regions where the cells were becoming deformed (Fig. 5), these results suggest that the degradation of PG is anisotropic in the $\Delta asnB$ mutant. Such degradation could result from either breakup (loss) of PG through PG hydrolase activity or from PG maturation. A key PG maturation enzyme in *B. subtilis* is the D,D-carboxypeptidase DacA, which removes the fifth amino acid from stem peptides and contributes to the loss of fluorescent D-amino acids after labeling of PG (Kuru *et al.*, 2015). Although spatial deregulation of DacA activity could explain the anisotropic loss of TDL in $\Delta asnB$ mutant cells, it could not account for the accompanying lysis and deformation phenotype. This phenotype requires the activity of PG hydrolases which would affect the connectivity of the PG meshwork and act on its structural bonds. Therefore, the lysis phenotype of $\Delta asnB$ and the associated loss of label in regions of cell deformation is consistent with deregulation of one, or a combination of, PG hydrolases. In conclusion, the absence of amidated mDAP and Mg^{2+} leads to anisotropic PG hydrolysis and associated morphological deformation, ultimately causing cell lysis.

Mg^{2+} inhibits cellular autolysis

We found that Mg^{2+} inhibited the lysis of the $\Delta asnB$ mutant, and it was also previously shown to prevent the lysis of $\Delta mreB$ mutants (Formstone and Errington, 2005). Furthermore, Mg^{2+} inhibits cell lysis induced by diverse conditions in unrelated Gram-negative microorganisms (Rayman and MacLeod, 1975; Leduc *et al.*, 1982; Gschwender and Hofschneider, 1969). Thus, we tested whether Mg^{2+} may have an inhibitory effect on PG hydrolases in *B. subtilis*. The autolysins responsible for cell lysis in *B. subtilis* are LytC, LytD, LytE and LytF (Jolliffe *et al.*, 1981). The rate of cell autolysis upon depolarization of the membrane by addition of

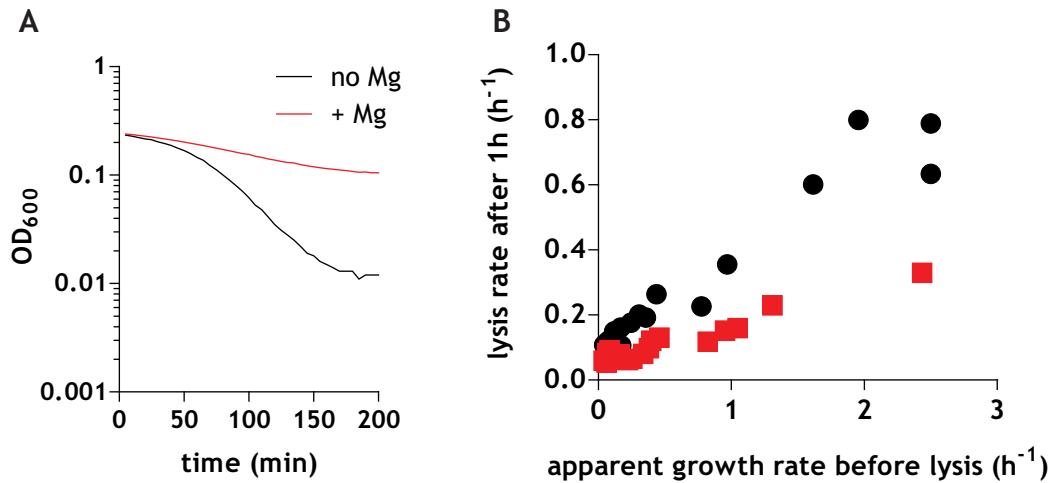


Fig. 7. Mg²⁺ reduces the rate of autolysis.

A. Rate of autolysis of wild-type strain grown to mid-exponential phase in the absence (black line) or in the presence (red line) of 25 mM MgSO₄ added to cultures at the same time as azide.

B. Apparent instantaneous growth rate of cells in various stages of exponential growth is plotted against their autolysis rate with (red squares) or without (black circles) 25 mM MgSO₄.

uncouplers can be therefore used as a readout of their activity.

Mg²⁺ reproducibly inhibited the rate of autolysis of wild-type cells (a typical autolysis curve for cells in mid-exponential growth is shown in Fig. 7A). We noticed that the rates of cell autolysis of wild-type *B. subtilis* reported in the literature are variable, and this variability was evident in our initial experiments. Thus, we hypothesized that the rate of autolysis is dependent on the phase of growth of the cells. We therefore examined it in various stages of growth, from the exit from the lag phase to entry into stationary phase (see Materials and Methods). To correlate it with the phase of growth, we measured the apparent instantaneous rate of growth of the cells five minutes before addition of the uncoupler and plotted it against the rate of lysis. This approach revealed a linear relationship between the apparent instantaneous growth rate of the cells and the rate of cell autolysis (Fig. 7B), possibly explaining the variability of the reported lysis rates in the literature. Importantly, the presence of 25 mM Mg²⁺ inhibited the rate of lysis at all stages of growth (Fig. 7B). This suggests that Mg²⁺ exerts an inhibitory effect on PG hydrolysis catalyzed by autolysins.

Increased sensitivity of the Δ asnB mutant to lysozyme and cell wall active antibiotics

Deregulation of the homeostasis of PG hydrolysis in the Δ asnB mutant, with the resulting imbalance between PG synthesis and degradation, could sensitize Δ asnB cells to perturbations of the cell wall, such as the action of

lysozyme and antibiotics that target the cell wall. Furthermore, PG hydrolysis has been implicated in the mechanism of action of many antibiotics that target the cell wall (Rogers *et al.*, 1983; Tomasz *et al.*, 1970; Goodell *et al.*, 1976; Luo and Helmann, 2012).

Presence of lysozyme in the growth medium totally inhibited the growth of Δ asnB mutant strain at concentrations (1 mg ml⁻¹) where the growth of the wild-type strain was unaffected (Fig. 8A). This increased sensitivity to lysozyme is consistent with the results obtained for the Δ ltsA mutant in *C. glutamicum* (Lefevaudes *et al.*, 2015).

We then used disk diffusion assays to compare the sensitivity of the Δ asnB mutant strain and the wild-type to various antibiotics targeting different cellular processes. As expected, the Δ asnB mutant was more sensitive than the wild-type to antibiotics which target different steps of cell wall synthesis, including D-cycloserine, vancomycin, tunicamycin, methicillin, penicillin and cefuroxime. It nevertheless had the same sensitivity as the wild-type strain to the DNA gyrase inhibitor ciprofloxacin, the RNA polymerase inhibitor rifampicin, and the uncoupler CCCP (Fig. 8B).

Discussion

Magnesium holds a very particular place in cell biology of *B. subtilis* since it can compensate the absence of a number of otherwise essential cell wall related genes. Hypotheses put forward to explain this effect include the idea that Mg²⁺ may somehow rigidify the cell wall, or that it may affect the activity of cell wall associated

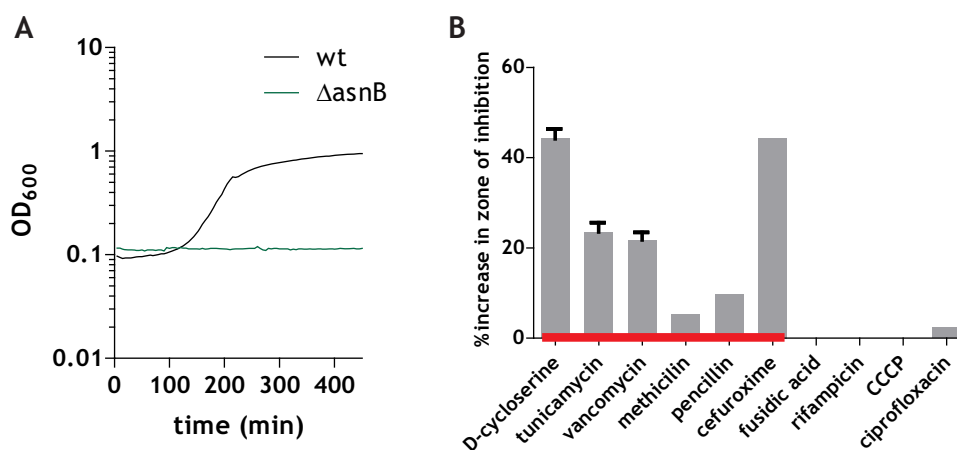


Fig. 8. Increased sensitivity of the $\Delta asnB$ mutant to lysozyme and antibiotics that target the cell wall.

A. Growth curves for wild-type (black line) and $\Delta asnB$ (green line) grown in LB (+25 mM $MgSO_4$) in the presence of 1 mg ml⁻¹ lysozyme. B. Results of disk diffusion assays with the indicated antibiotics. Bars indicate the percent increase in zone of inhibition for the $\Delta asnB$ mutant relative to the wild-type. Error bars are 95% confidence intervals (where not indicated, error bars are smaller than what can be represented graphically by the Prism plotting software).

enzymes, or both (Formstone and Errington, 2005). We have tested the effect of Mg^{2+} on the rigidity of the cell wall of wild-type *B. subtilis* cells using AFM and have found no effect. However, we identified a significant decrease in the degree of amidation of mDAP in cells grown in the presence of high concentrations (25 mM) of Mg^{2+} , but not in the presence of equivalent ionic strength of NaCl. Amidation of mDAP in *B. subtilis* has been known for a long time, but its significance has remained obscure. In *B. subtilis* and other species where it has been reported, mDAP amidation is extensive, but not total, and it seems to slightly differ in different growth conditions (Atrih *et al.*, 1999), suggesting a possible regulatory role in cell wall homeostasis (see also below).

We identified *asnB*, a gene encoding a member of glutamine amidotransferase family (Massiere and Badet-Denisot, 1998), as indispensable for this amidation. AsnB is predicted to be a cytoplasmic protein indicating that mDAP amidation occurs on peptidoglycan precursors inside the cell, consistent with previous results with *C. glutamicum* LtsA (Levefaudes *et al.*, 2015). Surprisingly, the $\Delta asnB$ mutant strain was only viable in the presence of high concentrations of Mg^{2+} . Under these conditions, the cells were shorter and wider, but their ultrastructure and mechanics were not different from wild-type. This width and length phenotype is similar to the phenotype of cells in which the DL-endopeptidase CwlO is inactivated (Meisner *et al.*, 2013; Salzberg *et al.*, 2013), evoking a possible disruption of normal functioning of the PG hydrolytic system in the $\Delta asnB$ mutant. Indeed, when the concentration of Mg^{2+} was lowered in the growth medium, $\Delta asnB$ mutant cells

began to deform and lyse, revealing the essential role of mDAP amidation in cell wall homeostasis.

We found that spatial organization of PG insertion is not affected in the $\Delta asnB$ mutant. In addition, the degree of crosslinking of peptide stems, which is a proxy for the activity of PG transpeptidases, was unchanged in $\Delta asnB$ relative to wild-type. Transpeptidases are therefore not affected by the absence amidated mDAP in *B. subtilis*, even though this amino acid participates in crosslinks. This is similar to the results obtained in *C. glutamicum* where the AsnB homologue LtsA has been shown not to be required for efficient transpeptidation activity (Levefaudes *et al.*, 2015).

In contrast to the normal spatial organization of PG insertion, the zones of PG degradation were anisotropically distributed in the $\Delta asnB$ mutant in the absence of excess Mg^{2+} . There were extensive zones of uncontrolled degradation that correlated with the zones of deformation from normal rod-shaped morphology. Thus, the genesis of the deformed morphology of $\Delta asnB$ mutant cells lies in the loss of homeostasis of PG hydrolysis. Uncontrolled regional PG hydrolysis leads to a disequilibrium between synthesis and degradation, causing deformation and, ultimately, lysis. This phenotype suggests a surprising degree of uncoupling between the synthetic and hydrolytic activities in this mutant when Mg^{2+} concentration is lowered.

It is generally accepted that the synthesis of new PG chains is somehow coupled with hydrolysis of the existing meshwork. According to the prevailing model, growth of the multilayered Gram-positive sacculi follows a push-up 'inside-to-outside' mechanism (Koch and Doyle, 1985), where new PG is inserted at the innermost face

of the sacculus, pushing outward pre-existing PG meshwork, which is then degraded and released into the medium by the action of PG hydrolases. The model is termed 'make before break' since the physiological coupling between synthesis and hydrolysis involves the polymerization and crosslinking of glycan chains prior to degradation (Koch *et al.*, 1981). In the absence of amidated mDAP and without excess Mg^{2+} uncontrolled hydrolysis occurs in the regions of the cell where we are able to detect orderly PG insertion. Our results therefore suggest that mDAP amidation allows physiological control over activity of one or more PG hydrolytic enzymes and their coupling with the PG synthetic machinery.

The masking of the $\Delta asnB$ lysis phenotype by Mg^{2+} indicates that this ion inhibits the lethal activity of certain PG hydrolases that become deregulated in the absence of amidated mDAP. The only PG hydrolases whose kinetics can be measured in whole cells are the autolysins, and we showed that Mg^{2+} indeed inhibits their activity. *B. subtilis* has a complement of about 40 putative PG hydrolases (Smith *et al.*, 2000), nearly twenty of which are expressed under vegetative growth conditions. However, it remains to be determined which of these PG hydrolases is inhibited by Mg^{2+} and which become deregulated in the absence of amidation of mDAP. Nevertheless, the effect of Mg^{2+} on inhibition of lysis has now been shown both in Gram-positive (present study) and in phylogenetically distant Gram-negative organisms (Gschwender and Hofschneider, 1969; Rayman and MacLeod, 1975; Leduc *et al.*, 1982), possibly suggesting the existence of a common inhibitory mechanism. The reported affinity of wild-type cell wall for Mg^{2+} is on the order of approximately 0.6 mM (Takahashi *et al.*, 2013; Kern *et al.*, 2010). At millimolar concentrations the vast majority of binding sites on the cell wall are occupied by Mg^{2+} . It is therefore unlikely that changing the concentration of Mg^{2+} in the medium from 5 to 10 mM significantly affects the degree of Mg^{2+} bound to cell wall polymers. Nevertheless, this is precisely the concentration range at which the $\Delta asnB$ mutant is rescued by Mg^{2+} . This suggests that the inhibitory activity of Mg^{2+} on PG hydrolases may not depend on its binding to cell wall polymers, but rather may be a result of direct interaction of Mg^{2+} with the enzymes. Further biochemical studies on purified enzymes will be necessary to elucidate this question.

Taken together, our data lead to a model in which *B. subtilis* modulates the degree of amidation of mDAP to maintain an appropriate balance between hydrolysis and degradation with changing environmental and physiological conditions. The changes in mDAP amidation induced in the wild-type cells by the presence of high concentrations of Mg^{2+} and the lysis phenotype of $\Delta asnB$ mutant are consistent with this model. Namely, since

Mg^{2+} acts as an inhibitor for certain PG hydrolases, excess Mg^{2+} in the medium affects the balance between hydrolysis and synthesis and causes it to shift toward decreased hydrolysis. The cell would in turn try to compensate to restore the balance by reducing the extent of amidation of mDAP. Since the expression of *asnB* is unaffected by the presence of added Mg^{2+} (our unpublished results), the physiological adaptation occurs through post-transcriptional means. The decrease in amidation would then permit the cell to increase the activity of hydrolytic enzymes to allow normal growth.

Finally, the altered homeostasis of PG hydrolysis in the $\Delta asnB$ mutant likely causes the observed increased sensitivity of the mutant cells to cell wall active antibiotics. Interestingly, mutants of the amidotransferase *ItsA* responsible for mDAP amidation in *C. glutamicum* also display higher susceptibility to β -lactam antibiotics (Lefebvre *et al.*, 2015). This suggests that amidation of mDAP could be used as a target for adjuvant antibiotic therapies aimed to increase the activity of existing antibiotics.

Experimental procedures

Genetics, strain construction and growth conditions

The strains used in this study are described in Supporting Information Table 3. Chromosomal DNA was prepared using the Promega Genomic DNA prep kit according to manufacturer's instructions. Standard genetics techniques were used for transformation (Marston and Errington, 1999). Selection of transformants was done on plates with or without 25 mM $MgSO_4$ as indicated in the text. The strains were verified by PCR. The antibiotic concentrations used were as follows: chloramphenicol 5 μ g/mL, erythromycin 1 μ g/mL, kanamycin 10 μ g/mL and spectinomycin 100 μ g/mL. Growth curves were done in 96-well plates in Synergy microplate reader (Biotek) with continuous agitation at 37°C. For all experiments, overnight cultures were diluted at least 10 000 in fresh medium and allowed to grow under conditions indicated in the text to early exponential phase before microscopic observation.

Peptidoglycan purification

B. subtilis wild-type and mutant strains were grown in 1 L cultures (in growth media indicated in the text) to $OD_{600} = 0.5$. Cultures were chilled in ice-ethanol bath for 20 min before harvesting by centrifugation at 5000g for 15 min at 4°C. Cell pellets were resuspended in 40 ml of ice cold water and slowly added to 40 ml of boiling 8% SDS. Cells were boiled for 30 minutes and allowed to cool before centrifugation and repeated (~15 times) washes with hot water to remove the SDS. The pellets were subsequently resuspended and incubated with 2 mg ml⁻¹ of Pronase (Roche) in 40 mM Tris-HCl (pH 7) at 60°C for 90 min. After

centrifugation, the pellets were washed with water and incubated with trypsin (Sigma) at $200 \mu\text{g ml}^{-1}$ in 20 mM Tris-HCl (pH 7.5) over night with agitation. Samples were boiled for 5 min and washed with water before treatment with DNAase ($10 \mu\text{g ml}^{-1}$) and RNAase ($50 \mu\text{g ml}^{-1}$) in 20 mM Tris-HCl pH 7, 20 mM MgCl_2 , 10 mM CaCl_2 for 2 hours at 37°C with agitation. SDS was added to the samples (1% final concentration) and the samples were incubated in boiling water for 15 min. Samples were washed 3 times with water and resuspended in 10 ml of 8 M LiCl, incubated for 15 min at 37°C and washed with water. The pellets were resuspended in 10 ml of 100 mM EDTA pH 7, incubated at 37°C for 15 min and washed with water. The pellets were resuspended in 10 ml acetone, sonicated for 5 min in ultrasonic bath, and washed with water three times. The samples were then resuspended in small volume of water and transferred to pre-weighed 2.2 ml tubes whose caps were punctured with a hot needle. The samples were lyophilized overnight and the purified cell wall weighed. The cell walls were resuspended to a final volume of 20 mg ml^{-1} and stored at -20°C .

To remove the teichoic acids and associated polymers, 10 mg of purified cell walls were incubated with 2 ml of concentrated hydrofluoric acid (46% HF) for 48 hours at 4°C . After this incubation, 15 ml of 100 mM Tris-HCl pH 7 was added to the sample and the samples were centrifuged and washed repeatedly with 100 mM Tris-HCl pH7 until the sample pH was neutral. The pellets were then washed three times with water and the pure PG was lyophilized overnight and then resuspended in water to 10 mg ml^{-1} .

Digestion of peptidoglycan with mutanolysin

To digest the purified peptidoglycan, $50 \mu\text{l}$ of pure peptidoglycan (10 mg ml^{-1}) was incubated in $50 \mu\text{l}$ of 25 mM NaH_2PO_4 pH 5.5 and $2 \mu\text{l}$ of mutanolysin (10 mg ml^{-1}) under agitation at 37°C overnight. After this incubation, $100 \mu\text{l}$ of water was added and the sample was boiled for 5 min to inactivate the enzyme. The sample was centrifuged and the muropeptides found in the supernatant were reduced with NaBH_4 ($200 \mu\text{l}$ of muropeptides solution, $200 \mu\text{l}$ 0.5 M borate buffer pH 9, $25 \mu\text{l}$ fresh NaBH_4 at 50 mg ml^{-1}) for 20 min at room temperature in open eppendorf tubes with occasional agitation to remove the bubbles of H_2 . The reduction reaction was ended by adjusting the sample pH to approximately 4 with 85% ortho-phosphoric acid.

UHPLC and mass spectrometry

Muropeptides resulting from mutanolysin digestion were separated by reverse phase ultrahigh-performance liquid chromatography using a Zorbax RRHD Eclipse Plus column (C18 $2.1 \times 100 \text{ mm}$ $1.8\text{-}\mu\text{m}$) at 50°C on Agilent UHPLC129 system. The buffers were at 10 mM ammonium phosphate, pH 5.6 (sodium azide at $180 \mu\text{g L}^{-1}$ was added to buffer A to avoid baseline drift at 202 nm). The methanol gradient (from 0% in buffer A to 20% in buffer B) was developed at a flow rate of 0.5 ml min^{-1} . Muropeptides were analyzed directly by matrix-assisted laser desorption/ionization-time of flight (MALDI-TOF) mass spectrometry, as previously described (Courtin *et al.*, 2006). The peaks

identified by MALDI-TOF were integrated in the Agilent software to estimate the amount of each muropeptide. The reported crosslinking index (%) was calculated as previously described (Glauner, 1988). The %dimers/(%monomers + $2 \times$ %dimers).

Labeling with TDL and microscopy

For TDL labeling, $100 \mu\text{l}$ of culture in early exponential phase was stained with 1 mM TDL (TAMRA Red D-lysine) at 37°C for 5 minutes (PG insertion labeling experiments) or 20 min (PG degradation pulse-chase experiments). Cells were rinsed twice in culture medium and $5 \mu\text{l}$ of washed cells deposited on 1% agarose pads poured in frames glued on microscope slides (Gene Frame from Thermo Scientific). The imaging was done on Zeiss Elyra PS1 using ZEN software. Cells were imaged in 3D-SIM mode with a $63\times$ objective, $0.12 \mu\text{m}$ z step (20 steps), 50 ms exposure time and 20% laser power (561 nm). Image reconstruction was performed in ZEN with automatic parameter setting.

Samples for phase contrast and epifluorescence microscopic observations were prepared as above and imaged by an inverted Nikon microscope (Ti-E) using a $100\times$ phase lens, or on Zeiss Elyra PS1 as above. For measurement of cell width and length, cells were incubated in the presence of FM4-64 ($1 \mu\text{g ml}^{-1}$). Cell width and length measurements were done in a custom program in MATLAB.

Microfluidics

Bacterial growth and pulse chase experiments using TDL dye were realized in the B04A Microfluidic Bacteria Plate (CellASIC ONIX, Millipore) using an Eclipse Ti-E inverted microscope (Nikon). Experiments were carried out at 37°C . Pressure setting of 5 psi was used to inject the medium into the growth chamber. For growth experiment, phase images were taken every 20 seconds. For TDL pulse-chase experiments, cells were grown in LB and stained for 20 min in LB + 1 mM TDL in the microfluidic device. Cells were then rinsed in fresh LB and images of phase and fluorescence were taken every 5 min.

Measurement of rate of autolysis

An overnight liquid culture of *B. subtilis* 168 grown in Difco Antibiotic Medium 3 (PAB) was diluted to an $\text{OD}_{600 \text{ nm}}$ of 1 and subsequently diluted by $\geq 10^4$ fold in PAB and incubated with continuous shaking at 37°C with $\text{OD}_{600 \text{ nm}}$ measurements being taken every five minutes. Cultures were set up in duplicate and grown to various stages of growth, including early, mid and late exponential phase at which point MgSO_4 was added to half of the cultures to a final concentration of 25 mM. Immediately after this addition autolysis was induced by adding sodium azide to all cultures at a final concentration of 75 mM. The $\text{OD}_{600 \text{ nm}}$ was monitored to follow the rate of lysis. To determine the apparent growth rate μ just before adding the uncoupler, we selected the last 20 min (5 time points) of the log-normalized growth curves, and applied a standard least-squares linear fit. Similarly, we applied the same regression

to the first hour (12 time points) of the log-normalized lysis curves to obtain the lysis rates reported in Fig. 7.

Sample preparation for AFM

Overnight cultures of the indicated strains were diluted into fresh LB (containing or not 25 mM MgSO₄) and grown at 37°C. When cells reached OD₆₀₀ ~ 0.4, 1 ml of culture was harvested and allowed to settle for 20 min on a piranha cleaned, cell-tak modified (Corning), glass bottom Petri dish (WPI, Meyer *et al.*, 2010). Unattached cells were washed away and the attached cells covered with culture medium for further analysis with AFM.

Atomic force microscopy

Imaging and force measurement were realized using a Nanowizard 3 Atomic Force Microscope (JPK Instruments AG, Berlin, Germany) coupled to a Zeiss inverted microscope. Topographic images and elasticity cartography were generated simultaneously using the Quantitative Imaging® (QI) mode with DNP cantilevers (0.06–0.24 N m⁻¹, Bruker) in culture medium. The ramp size and speed were set at 400 μm and 25 μm s⁻¹ respectively and the maximum load was 6 μN, maps of 128 by 128 force curves were realized. Calibration of the probe was carried out by measuring the deflection sensitivity on glass surface and spring constant was determined using the thermal tune method. Young moduli were calculated by fitting force curves with the Sneddon model using the JPK software.

Electron microscopy

For transmission electron microscopy (TEM), cells were harvested at the desired OD₆₀₀ by centrifugation, washed two times with PBS and fixed in 2% glutaraldehyde and 0.1 M sodium cacodylate buffer pH 7.2, for 2 h at room temperature. Subsequent steps were performed mainly as described in (Rueff *et al.*, 2014). TEM observations were done at the Microscopy and Imaging Platform MIMA2, INRA of Jouy-en-Josas, France.

Disk diffusion assays

Disk diffusion assays were performed as follows. Petri plates containing LB medium were covered with 5 ml of soft agar in which 200 μl of exponentially growing cells (OD₆₀₀ = 0.2–0.4) of the strain being tested were resuspended. The plates were allowed to dry briefly in a laminar flow hood before 6 mm paper disks (Whatman) containing 25 μl of antibiotic solution were placed on the disks (cefuroxime 8 mg ml⁻¹, ciprofloxacin 100 μg ml⁻¹, D-cycloserine 16 mg ml⁻¹, CCCP 2.25 mg ml⁻¹, fusidic acid, 12.8 μg ml⁻¹, methicillin 12.5 mg ml⁻¹, penicillin 8 mg ml⁻¹, rifampicin 128 μg ml⁻¹, tunicamycin 375 μg ml⁻¹, vancomycin 0.5 μg ml⁻¹). The plates were incubated at 37°C overnight and the zones of inhibition were measured by ImageJ after scanning the plates. Two disks were used per antibiotic and per plate. The values reported in Fig. 8 are an average of three independent experiments.

Acknowledgements

We thank Yves Brun, Michael Van Nieuwenhze, and Erkin Kuru for the gift of TDL; Ken-Ichi Yoshida for the gifts of strains FU340, FU341 and FU342. We thank Christine Longin from the Microscopy and Imaging Platform MIMA2 (INRA, France) for help with TEM observations. MS data were obtained with the instruments located at the INRA Platform for Proteomics Analysis of Paris South West (PAPPSO) and the Mass Spectrometry Laboratory, Analytical Services Unit, Instituto de Tecnologia Química e Biológica, Universidade Nova de Lisboa. The authors declare no conflict of interest.

Funding information

This work was supported by a starting grant from the European Research Council to R.C.-L. (ERC-StG 311231). B. Tesson was supported by Marie Skłodowska Curie Individual Fellowship BACTOSHAPE 660935. P. Flores was supported by a doctoral fellowship from INRA.

Author contributions

A.D. conceived the study; A.D., B.T., S.C., P.C., R.K. performed the experiments; A.D., B.T., P.C., P.F. and M.C.-C. analyzed the data; S.F., C.M., M.C.-C. contributed equipment and training, A.D., B.T. and R.C.L. wrote the article.

References

- Asong, J., Wolfert, M.A., Maiti, K.K., Miller, D., and Boons, G.J. (2009) Binding and cellular activation studies reveal that toll-like receptor 2 can differentially recognize peptidoglycan from gram-positive and gram-negative bacteria. *J Biol Chem* **284**: 8643–8653.
- Atrih, A., Bacher, G., Allmaier, G., Williamson, M.P., and Foster, S.J. (1999) Analysis of peptidoglycan structure from vegetative cells of *Bacillus subtilis* 168 and role of PBP 5 in peptidoglycan maturation. *J Bacteriol* **181**: 3956–3966.
- Bernard, E., Rolain, T., Courtin, P., Guillot, A., Langella, P., Hols, P., and Chapot-Chartier, M.P. (2011a) Characterization of O-acetylation of N-acetylglucosamine: a novel structural variation of bacterial peptidoglycan. *J Biol Chem* **286**: 23950–23958.
- Bernard, E., Rolain, T., Courtin, P., Hols, P., and Chapot-Chartier, M.P. (2011b) Identification of the amidotransferase AsnB1 as being responsible for meso-diaminopimelic acid amidation in *Lactobacillus plantarum* peptidoglycan. *J Bacteriol* **193**: 6323–6330.
- Beveridge, T.J., and Murray, R.G. (1980) Sites of metal deposition in the cell wall of *Bacillus subtilis*. *J Bacteriol* **141**: 876–887.

- Brown, S., Santa Maria, J.P., Jr., and Walker, S. (2013) Wall teichoic acids of gram-positive bacteria. *Annu Rev Microbiol* **67**: 313–336.
- Chastanet, A., and Carballido-Lopez, R. (2012) The actin-like MreB proteins in *Bacillus subtilis*: a new turn. *Front Biosci (Schol Ed)* **4**: 1582–1606.
- Courtin, P., Miranda, G., Guillot, A., Wessner, F., Mezange, C., Domakova, E., Kulakauskas, S., and Chapot-Chartier, M.P. (2006) Peptidoglycan structure analysis of *Lactococcus lactis* reveals the presence of an L, D-carboxypeptidase involved in peptidoglycan maturation. *J Bacteriol* **188**: 5293–5298.
- Davis, K.M., and Weiser, J.N. (2011) Modifications to the peptidoglycan backbone help bacteria to establish infection. *Infect Immun* **79**: 562–570.
- Dominguez-Escobar, J., Chastanet, A., Crevenna, A.H., Fromion, V., Wedlich-Soldner, R., and Carballido-Lopez, R. (2011) Processive movement of MreB-associated cell wall biosynthetic complexes in bacteria. *Science* **333**: 225–228.
- Eun, Y.J., Kapoor, M., Hussain, S., and Garner, E.C. (2015) Bacterial filament systems: toward understanding their emergent behavior and cellular functions. *J Biol Chem* **290**: 17181–17189.
- Figueiredo, T.A., Sobral, R.G., Ludovice, A.M., Almeida, J.M., Bui, N.K., Vollmer, W., de Lencastre, H., and Tomasz, A. (2012) Identification of genetic determinants and enzymes involved with the amidation of glutamic acid residues in the peptidoglycan of *Staphylococcus aureus*. *PLoS Pathog* **8**: e1002508.
- Formstone, A., and Errington, J. (2005) A magnesium-dependent mreB null mutant: implications for the role of mreB in *Bacillus subtilis*. *Mol Microbiol* **55**: 1646–1657.
- Garner, E.C., Bernard, R., Wang, W., Zhuang, X., Rudner, D.Z., and Mitchison, T. (2011) Coupled, circumferential motions of the cell wall synthesis machinery and MreB filaments in *B. subtilis*. *Science* **333**: 222–225.
- Girardin, S.E., Travassos, L.H., Herve, M., Blanot, D., Boneca, I.G., Philpott, D.J., Sansonetti, P.J., and Mengin-Lecreulx, D. (2003) Peptidoglycan molecular requirements allowing detection by Nod1 and Nod2. *J Biol Chem* **278**: 41702–41708.
- Glauner, B. (1988) Separation and quantification of muropeptides with high-performance liquid chromatography. *Anal Biochem* **172**: 451–464.
- Goodell, E.W., Lopez, R., and Tomasz, A. (1976) Suppression of lytic effect of beta lactams on *Escherichia coli* and other bacteria. *Proc Natl Acad Sci U S A* **73**: 3293–3297.
- Gschwender, H.H., and Hofschneider, P.H. (1969) Lysis inhibition of phi-X174-, M12-, and Q-beta-infected *Escherichia coli* bacteria by magnesium ions. *Biochim Biophys Acta* **190**: 454–459.
- Heckels, J.E., Lambert, P.A., and Baddiley, J. (1977) Binding of magnesium ions to cell walls of *Bacillus subtilis* W23 containing teichoic acid or teichuronic acid. *Biochem J* **162**: 359–365.
- Hirasawa, T., Wachi, M., and Nagai, K. (2000) A mutation in the *Corynebacterium glutamicum* ItsA gene causes susceptibility to lysozyme, temperature-sensitive growth, and L-glutamate production. *J Bacteriol* **182**: 2696–2701.
- Huang, X., Holden, H.M., and Raushel, F.M. (2001) Channeling of substrates and intermediates in enzyme-catalyzed reactions. *Annu Rev Biochem* **70**: 149–180.
- Jolliffe, L.K., Doyle, R.J., and Streips, U.N. (1981) The energized membrane and cellular autolysis in *Bacillus subtilis*. *Cell* **25**: 753–763.
- Kern, T., Giffard, M., Hediger, S., Amoroso, A., Giustini, C., Bui, N.K., Joris, B., Bougault, C., Vollmer, W., and Simorre, J.P. (2010) Dynamics characterization of fully hydrated bacterial cell walls by solid-state NMR: evidence for cooperative binding of metal ions. *J Am Chem Soc* **132**: 10911–10919.
- Koch, A.L., and Doyle, R.J. (1985) Inside-to-outside growth and turnover of the wall of gram-positive rods. *J Theor Biol* **117**: 137–157.
- Koch, A.L., Higgins, M.L., and Doyle, R.J. (1981) Surface tension-like forces determine bacterial shapes: *Streptococcus faecium*. *J Gen Microbiol* **123**: 151–161.
- Kuru, E., Hughes, H.V., Brown, P.J., Hall, E., Tekkam, S., Cava, F., de Pedro, M.A., Brun, Y.V., and VanNieuwenhze, M.S. (2012) In Situ probing of newly synthesized peptidoglycan in live bacteria with fluorescent D-amino acids. *Angew Chem Int Ed Engl* **51**: 12519–12523.
- Kuru, E., Tekkam, S., Hall, E., Brun, Y.V., and Van Nieuwenhze, M.S. (2015) Synthesis of fluorescent D-amino acids and their use for probing peptidoglycan synthesis and bacterial growth in situ. *Nat Protoc* **10**: 33–52.
- Lamsa, A., Liu, W.T., Dorrestein, P.C., and Pogliano, K. (2012) The *Bacillus subtilis* cannibalism toxin SDP collapses the proton motive force and induces autolysis. *Mol Microbiol* **84**: 486–500.
- Leduc, M., Kasra, R., and van Heijenoort, J. (1982) Induction and control of the autolytic system of *Escherichia coli*. *J Bacteriol* **152**: 26–34.
- Levefaudes, M., Patin, D., de Sousa-D'auria, C., Chami, M., Blanot, D., Herve, M., Arthur, M., Houssin, C., and Mengin-Lecreulx, D. (2015) Diaminopimelic Acid Amidation in *Corynebacteriales*: new insights into the role of Itsa in peptidoglycan modification. *J Biol Chem* **290**: 13079–13094.
- Luo, Y., and Helmann, J.D. (2012) Analysis of the role of *Bacillus subtilis* sigma(M) in beta-lactam resistance reveals an essential role for c-di-AMP in peptidoglycan homeostasis. *Mol Microbiol* **83**: 623–639.
- Mahapatra, S., Yagi, T., Belisle, J.T., Espinosa, B.J., Hill, P.J., McNeil, M.R., Brennan, P.J., and Crick, D.C. (2005) Mycobacterial lipid II is composed of a complex mixture of modified muramyl and peptide moieties linked to decaprenyl phosphate. *J Bacteriol* **187**: 2747–2757.
- Marston, A.L., and Errington, J. (1999) Selection of the midcell division site in *Bacillus subtilis* through MinD-dependent polar localization and activation of MinC. *Mol Microbiol* **33**(1): 84–96.
- Massiere, F., and Badet-Denisot, M.A. (1998) The mechanism of glutamine-dependent amidotransferases. *Cell Mol Life Sci* **54**: 205–222.
- Meisner, J., Montero Llopis, P., Sham, L.T., Garner, E., Bernhardt, T.G., and Rudner, D.Z. (2013) FtsEX is required for CwlO peptidoglycan hydrolase activity during cell wall elongation in *Bacillus subtilis*. *Mol Microbiol* **89**: 1069–1083.

- Mesnage, S., Dellarole, M., Baxter, N.J., Rouget, J.B., Dimitrov, J.D., Wang, N., Fujimoto, Y., Hounslow, A.M., Lacroix-Desmazes, S., Fukase, K., Foster, S.J., and Williamson, M.P. (2014) Molecular basis for bacterial peptidoglycan recognition by LysM domains. *Nat Commun* **5**: 4269.
- Meyer, P., Gutierrez, J., Pogliano, K., and Dworkin, J. (2010) Cell wall synthesis is necessary for membrane dynamics during sporulation of *Bacillus subtilis*. *Mol Microbiol* **76**(4): 956–970.
- Munch, D., Roemer, T., Lee, S., Engeser, H.M., Sahl, H.G., and Schneider, T. (2012) Identification and in vitro analysis of the GatD/MurT enzyme-complex catalyzing lipid II amidation in *Staphylococcus aureus*. *PLoS Pathog* **8**: e1002509.
- Murray, T., Popham, D.L., and Setlow, P. (1998) *Bacillus subtilis* cells lacking penicillin-binding protein 1 require increased levels of divalent cations for growth. *J Bacteriol* **180**: 4555–4563.
- Neuhaus, F.C., and Baddiley, J. (2003) A continuum of anionic charge: structures and functions of D-alanyl-teichoic acids in gram-positive bacteria. *Microbiol Mol Biol Rev* **67**: 686–723.
- Nicolas, P., Mader, U., Dervyn, E., Rochat, T., Leduc, A., Pigeonneau, N., et al. (2012) Condition-dependent transcriptome reveals high-level regulatory architecture in *Bacillus subtilis*. *Science* **335**: 1103–1106.
- Raushel, F.M., Thoden, J.B., and Holden, H.M. (1999) The amidotransferase family of enzymes: molecular machines for the production and delivery of ammonia. *Biochemistry* **38**: 7891–7899.
- Rayman, M.K., and MacLeod, R.A. (1975) Interaction of Mg²⁺ with peptidoglycan and its relation to the prevention of lysis of a marine pseudomonad. *J Bacteriol* **122**: 650–659.
- Rogers, H.J., Thurman, P.F., and Burdett, I.D. (1983) The bactericidal action of beta-lactam antibiotics on an autolysin-deficient strain of *Bacillus subtilis*. *J Gen Microbiol* **129**: 465–478.
- Rueff, A.S., Chastanet, A., Dominguez-Escobar, J., Yao, Z., Yates, J., Prejean, M.V., et al. (2014) An early cytoplasmic step of peptidoglycan synthesis is associated to MreB in *Bacillus subtilis*. *Mol Microbiol* **91**: 348–362.
- Salzberg, L.I., Powell, L., Hokamp, K., Botella, E., Noone, D., and Devine, K.M. (2013) The WalRK (YycFG) and sigma(I) RsgI regulators cooperate to control CwlO and LytE expression in exponentially growing and stressed *Bacillus subtilis* cells. *Mol Microbiol* **87**: 180–195.
- Schleifer, K.H., and Kandler, O. (1972) Peptidoglycan types of bacterial cell walls and their taxonomic implications. *Bacteriol Rev* **36**: 407–477.
- Smith, T.J., Blackman, S.A., and Foster, S.J. (2000) Autolysins of *Bacillus subtilis*: multiple enzymes with multiple functions. *Microbiology* **146**: 249–262.
- Takahashi, H., Ayala, I., Bardet, M., De Paepe, G., Simorre, J.P., and Hediger, S. (2013) Solid-state NMR on bacterial cells: selective cell wall signal enhancement and resolution improvement using dynamic nuclear polarization. *J Am Chem Soc* **135**: 5105–5110.
- Tomasz, A., Albino, A., and Zanati, E. (1970) Multiple antibiotic resistance in a bacterium with suppressed autolytic system. *Nature* **227**: 138–140.
- Turner, R.D., Vollmer, W., and Foster, S.J. (2014) Different walls for rods and balls: the diversity of peptidoglycan. *Mol Microbiol* **91**: 862–874.
- Vollmer, W., Blanot, D., and de Pedro, M.A. (2008a) Peptidoglycan structure and architecture. *FEMS Microbiol Rev* **32**: 149–167.
- Vollmer, W., Joris, B., Charlier, P., and Foster, S. (2008b) Bacterial peptidoglycan (murein) hydrolases. *FEMS Microbiol Rev* **32**: 259–286.
- Warth, A.D., and Strominger, J.L. (1971) Structure of the peptidoglycan from vegetative cell walls of *Bacillus subtilis*. *Biochemistry* **10**: 4349–4358.
- Yamamoto, H., Miyake, Y., Hisaoka, M., Kurosawa, S., and Sekiguchi, J. (2008) The major and minor wall teichoic acids prevent the sidewall localization of vegetative DL-endopeptidase LytF in *Bacillus subtilis*. *Mol Microbiol* **70**: 297–310.
- Yoshida, K., Fujita, Y., and Ehrlich, S.D. (1999) Three asparagine synthetase genes of *Bacillus subtilis*. *J Bacteriol* **181**: 6081–6091.

Supporting information

Additional supporting information may be found in the online version of this article at the publisher's web-site.